JOURNAL OF AIRCRAFT
Vol. 34, No. 2, March–April 1997

# Low-Speed Wall Interference Assessment/Correction with Vortex Flow Effect

Ching-Chyuan A. Hsing* and C. Edward Lan†
*University of Kansas, Lawrence, Kansas 66045*

**A theoretical method based on the concept of wall pressure signatures for assessment/correction of wind-tunnel wall interference is presented. The effect of the tunnel wall in upflow and blockage corrections is evaluated by using a thin-layer Navier–Stokes solver. The results for a 65-deg delta wing and a wing–body–strake configuration in subsonic flow are presented. The present prediction of the effects of wall interference on the induced aerodynamic twist and the streamline curvature for the delta wing show a larger magnitude than those by a free vortex sheet method. Two correction charts for the upflow and blockage corrections for configurations with vortex flow are derived based on the computed results for the wing–body–strake configuration at a Mach number of 0.3. The present method shows consistent corrected results for different model sizes. In general, for a model with strong vortex flow, the present method provides larger corrections than the conventional attached flow theory. The present method can also provide guidelines on where the wall static pressures should be measured in the pressure signature method.**

## Nomenclature

| | | |
|---|---|---|
| $a$ | = | local speed of sound |
| $C$ | = | tunnel cross-sectional area |
| $C_D$ | = | drag coefficient |
| $C_L$ | = | lift coefficient |
| $C_m$ | = | pitching moment coefficient |
| $C_p$ | = | pressure coefficient |
| $E$ | = | total energy |
| $H$ | = | wind-tunnel height |
| ICP | = | interference correction parameter, Eq. (6) |
| $p$ | = | static pressure |
| $q$ | = | dynamic pressure |
| $S$ | = | wing planform area |
| $U_\infty$ | = | freestream velocity |
| $u$, $v$, $w$ | = | $x$, $y$, and $z$ velocity components |
| $W$ | = | wind-tunnel width |
| $x$, $y$, $z$ | = | Cartesian coordinates |
| $y^+$ | = | $(\rho_w \tau_w y)^{1/2}/\mu_w$ |
| $\alpha$ | = | angle of attack |
| $\beta$ | = | parameter controlling grid point spacing |
| $\mu$ | = | coefficient of viscosity |
| $\xi$, $\eta$, $\zeta$ | = | curvilinear coordinates |
| $\rho$ | = | density |
| $\tau$ | = | shear stress |

*Subscripts*

| | | |
|---|---|---|
| $c$ | = | corrected value |
| $w$ | = | wall |
| $\infty$ | = | property at freestream conditions |

## Introduction

TO obtain good quality and reliable wind-tunnel test data, factors related to wall interference, flow angularity, local variations in velocity, and support interference, etc., must be evaluated and corrected. Among these factors the wall interference effect is the subject of this paper. Because of the presence of the solid tunnel wall, the flow conditions around the model are usually different from those in the free-air condition. These differences may result in a reduction in the average downwash experienced by the model, in a change in the streamline curvature about the model, in an alteration to the local angle of attack along the span of the model, in a change in dynamic pressure about the model because of the solid and wake blockage, and in the buoyancy effect because of the axial pressure gradient in the test section. Especially for large models, the wall interference is expected to be very significant. In addition, in high-angle-of-attack aerodynamics with vortex flow, the wall interference may become an influential factor for the wind-tunnel data correction because of flow separation.

The classical procedure of correcting wall interference effects is based on the linear theory[1–3] by using the image method. The model is represented by singularities deduced from the model geometry and measured forces to correct the angle of attack. More recently, the vortex lattice method was used for closed test sections[4,5] and open test sections.[6] For the solid body and wake blockage corrections, Maskell[7] developed a method based on the measured drag coefficient. The method was improved by Pass.[8] Although these classical wall interference methods provide insight into the features of wall interference, they are not sufficient in producing accurate results for practical use at high angles of attack, in particular involving vortex flow. Also, it has several limitations, among them being the assumption that the model is small compared to the tunnel size and the assumption of an infinitely long test section, etc.

To eliminate some of the limitations of the classical theory, the so-called pressure signature method[9–11] has been developed in the past couple of years. This method uses the measured static pressures on the tunnel wall surfaces to obtain the necessary corrections. One main question in carrying out the wall pressure measurement is the determination of appropriate locations to make the measurements and the number of measuring points needed for an accurate evaluation. Furthermore, it is also a fact that frequently there exists significant discrepancy between data taken for the same model in different wind tunnels.

To avoid experimental measurement of wall pressures, theoretical methods have also been studied recently. Panel methods were used for three-dimensional subsonic wind tunnels[12,13] in the low-angle-of-attack range. Frink[14] used a free-vortex-sheet (FVS) method to calculate the wall effects for delta wings in subsonic flow. Although the vortex-separated flow at

Received July 29, 1996; revision received Dec. 1, 1996; accepted for publication Dec. 13, 1996. 

*Graduate Assistant, Department of Aerospace Engineering; currently President, Unicom Technology Systems, Lawrence, KS 66044.

†Bellows Distinguished Professor, Department of Aerospace Engineering. Associate Fellow AIAA.

high angle of attack was considered in predicting the interference corrections, no blockage or streamline curvature corrections were included.

High-order methods of computational fluid dynamics have also been used in the prediction of wind-tunnel wall interference. Rizk and Smithmeyer[15] reported a procedure to evaluate the Mach number and angle-of-attack corrections by solving the Laplace equation based on experimental pressure measurement. Vatsa and Wedan[16] used an unsteady Navier–Stokes solver to calculate the effect of sidewall boundary layer on a swept wing mounted in a wind tunnel. It showed good agreement of $C_p$ distributions and streamline patterns with experimental data for the case studied, but provided no corrections for force data.

Thomas and Lan[17] used a thin-layer Navier–Stokes solver to simulate a delta wing in a small tunnel. The computed wall $C_p$ was used as the boundary condition to calculate the wall-induced interference flowfield at the model location in the tunnel. The corrected lift curve showed good agreement with results from larger tunnels. Lan and Hsing[18] used the same method to simulate a wing–body–strake configuration tested in a 7 by 10 ft wind tunnel. The results showed that the corrections based on the computation provided adequate treatment for vortex flow in wall interference simulations.

To avoid large corrections, generally one of the following methods is adopted: reducing the model size, using very large test sections, ventilated test sections, or the adaptive wall concept. Conventionally, the wall interference correction for small models in terms of model blockage ratio, i.e., the model planform area to tunnel cross-sectional area ratio, is assumed to be small. According to Lefebvre,[19] the span of a straight wing should not exceed 75% of the tunnel width. For swept wings with a blockage ratio less than 0.08, tunnel interference can usually be considered negligible.[20] However, using a large model in the high-angle-of-attack testing is considered desirable in getting correct results[21] because geometry can be more accurately duplicated in detail.

Increasing the model size and angle of attack leads to an increase in the necessary corrections. Under these circumstances a conventional method can no longer provide adequate corrections needed for the measured data. Therefore, a reliable and inexpensive way for the assessment and correction of wall interference is very much needed. Ideally, the correction method should be independent of the model or tunnel size. One objective of this paper is to develop a method to fill this need by deriving correction charts for wall-induced upflow and blockage corrections in subsonic testing involving vortex flow. Solid wall surfaces are assumed throughout.

## Theoretical Method

In the present investigation, a thin-layer Navier–Stokes solver is used to obtain not only the angle-of-attack and streamline curvature corrections, but also the blockage corrections. The Navier–Stokes computational method and interference correction procedures are summarized in the following. More details about the computational method can be found in Refs. 17 and 18.

### Navier–Stokes Method

The flow solver used for the present study is based on a modified ARC3D code[22] with a two-block scheme of grid system for the purpose of tunnel simulation. The code is based on the three-dimensional Reynolds-averaged Navier–Stokes equations with a thin-layer approximation. The empirical turbulence model proposed by Balwin and Lomax[23] is used in the code. To effectively include the turbulent effect in the computation, the value of $y^+$ of the first grid line away from the solid surface should be typically less than 10. In the present computation, the value is usually in the range of 1.5–3.5. This requires a dense grid clustered to the body surface and the tunnel wall surface. This is accomplished by a coordinate

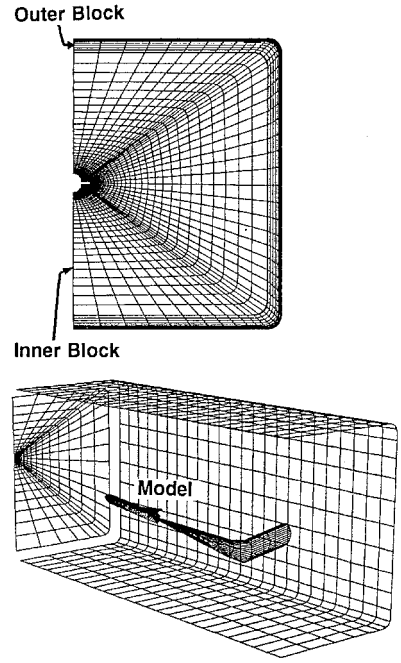


**Fig. 1 Two-block grid system used in the present method.**

stretching transformation being applied in the $\zeta$ direction. The stretching transformation is of the following form[24]:

$$\zeta(\omega) = 1 - \frac{\tanh[\sigma(1 - \omega)]}{\tanh \sigma} \tag{1}$$

where $\omega$ varies uniformly from 0 to 1, and $\sigma$ is given by the solution to

$$\beta = 1/\tanh \sigma \tag{2}$$

in which $\beta$ is a parameter close to 1, but is greater than 1. All grids used in this study employ a stretching parameter of $\beta = 1.005$. For the cases studied, the grid size used is $50 \times 49 \times 50$ in the inner block for the streamwise $\xi$, spanwise $\eta$, and surface-normal $\zeta$ directions, respectively. On the other hand the grid size used for the outer tunnel block is $50 \times 49 \times 16$, respectively. A typical grid system used is presented in Fig. 1.

### Boundary Conditions

The upstream and downstream boundaries in the computational domain are typically located two body lengths away from the body nose and tail, respectively. In the wing alone case, the distance is two wing root-chord lengths. In the simulation of tunnel flow, the boundary conditions at the upstream and downstream boundaries are similar to those of the far field in free air. In particular, at the downstream boundary only the static pressure is specified as the freestream value and the total pressure and other flow variables are computed as part of the solution. On solid surfaces, all velocity components are set to zero to satisfy the usual no-slip assumption. At the interface of model and wall layer regions (the inner and outer computational blocks), all flow variables are extrapolated to the boundary when the velocity is outward. When the velocity is inward, only the static pressure is extrapolated to ensure the continuity of pressure distribution. Use of local one-dimensional Riemann invariants to determine the boundary values was investigated and produced essentially the same results.[17]

### Interference Flowfield

The present method of determining the interference corrections is similar to that of the pressure signature method, except

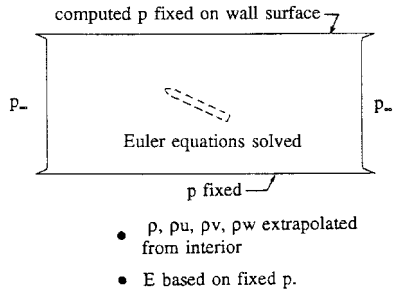


**Fig. 2 Illustration of calculation of interference flowfield.**

that the wall pressure distribution is calculated with the Navier–Stokes solver, instead of being measured. In addition, the calculated wall pressure distribution is used as the boundary data for a Euler resimulation of the tunnel domain with the model removed (Fig. 2). That is, the calculated wall pressure is specified on the wall surface and acts as the forcing function to generate the wall-induced flowfield in the test section by solving the Euler equations. This is done iteratively by extrapolating the interior values of density and flow momentum and calculating total energy based on the specified pressure on the boundary surfaces. This produces an interference flowfield that is compatible with the specified pressure distribution on the entire enclosed surface of the test section and contains information on $\Delta\alpha$, $\Delta u$, and $\Delta w$ that can be used to correct the measured tunnel data. In a conventional pressure signature method, this interference flowfield is usually generated by using a vortex or doublet distribution on the wall with the singularity strength determined with the measured wall pressure. The upflow correction is determined from

$$\alpha_c = \alpha + \Delta\alpha \tag{3}$$

where

$$\Delta\alpha = \tan^{-1}[\Delta w/(U_\infty + \Delta u)] \tag{4}$$

The correction to dynamic pressure is determined from

$$\frac{q_c}{q_\infty} = \frac{\rho[(U_\infty + \Delta u)^2 + \Delta w^2]}{\rho_\infty U_\infty^2} \tag{5}$$

**Wall Interference Corrections**

The present methodology to assess the effect of the wall interference is performed in two steps. The first step is to calculate by a Navier–Stokes flow solver the flowfield around a model in the tunnel to obtain the longitudinal characteristics, $C_L$, $C_D$, and $C_m$, along with the pressure distributions on the solid wall surfaces. The predicted wall pressures are then used to determine the interference flowfield. A flow blockage correction factor is calculated in this step with Eq. (5). However, the variables in Eqs. (4) and (5) vary across the flowfield. To correct the measured total aerodynamic forces and moments, the induced upflow variation along the span (Eq. 4) is computed in the far field over the wake region near the center plane. The final upflow correction to be used is taken as the average of these variations. The average blockage correction (Eq. 5) is always calculated at the end of the model, either at the body tail or at the wing trailing edge for a wing-alone case.

The correction procedures are outlined as follows:

1) $C_L$, $C_D$, and $C_m$ are first corrected for the blockage effect by dividing the measured values by the blockage factor [Eq. (5)] at the uncorrected test angle of attack.

2) The angle of attack is corrected to account for the upflow effect induced by the wall, by adding the upflow correction [Eq. (4)].

3) The final corrected $C_L$ and $C_D$ vs $\alpha$ curves are obtained by plotting the corrected $C_L$ and $C_D$ (step 1) at the corrected $\alpha$ (step 2).

4) The $C_m$ correction because of the upflow is calculated as the value of $(\Delta C_m/\Delta\alpha')\Delta\alpha$, where $\Delta C_m$ is the difference between the corrected $C_m$ from step 1 between two test $\alpha$, and $\Delta\alpha'$ is the difference between these test $\alpha$, and $\Delta\alpha$ is the upflow value obtained in step 2. The upflow correction for $C_m$ is then added to $C_m$ obtained in step 1.

## Results and Discussion

Results from the present method will first be compared with known results for a 65-deg delta wing.[14] The method will then be applied to the same delta wing and a wing–body–strake configuration to assess the wall interference effect on wall pressure signatures. Finally, wall interference corrections will be considered. The present code will be referred to as KUNS3D in all figures.

**65-Deg Delta Wing**

The calculations are made at a Mach number of 0.22 and a Reynolds number of $10^6$ for different model sizes with the span/tunnel-width ratios of 0.444, 0.5, and 0.667. The tunnel size is 117.4 × 46.96 in. and the wing area is 525.975 in.$^2$. Support interference is not included. The effect of model size on the aerodynamic twist is shown in Fig. 3. The induced upflow angles are obtained at the mid-root chord and Frink's results[14] are based on the free vortex sheet method. At $\alpha$ = 15 deg, the present results give higher values of the upflow angle, but the trend of the aerodynamic twist and the effect of the model size all agree with Frink's results.[14] At $\alpha$ = 30 deg, the present results are closer to Frink's,[14] though still slightly higher in magnitude. The trend again agrees well.

As shown in Fig. 4, the effect of model size on the streamline curvature predicted by the present method is compared with the results by Frink.[14] At $\alpha$ = 15 deg, the present calculation shows that the upflow agrees well in trend, but is again

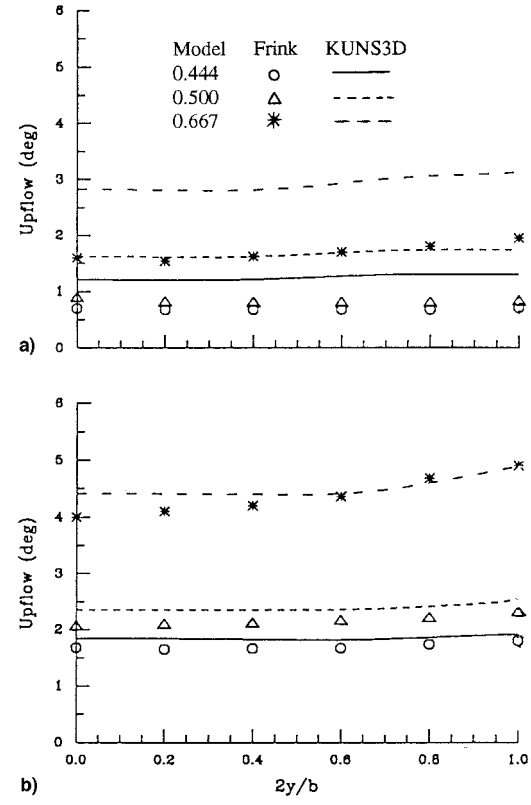


**Fig. 3 Effect of model-to-tunnel span ratios on the induced aerodynamic twist for a 65-deg delta wing in a 117.4 × 46.96 in. tunnel, $x/c_r$ = 0.5, $M$ = 0.22. Model scale = wing span/tunnel width ratio. $\alpha$ = a) 15 and b) 30 deg.**

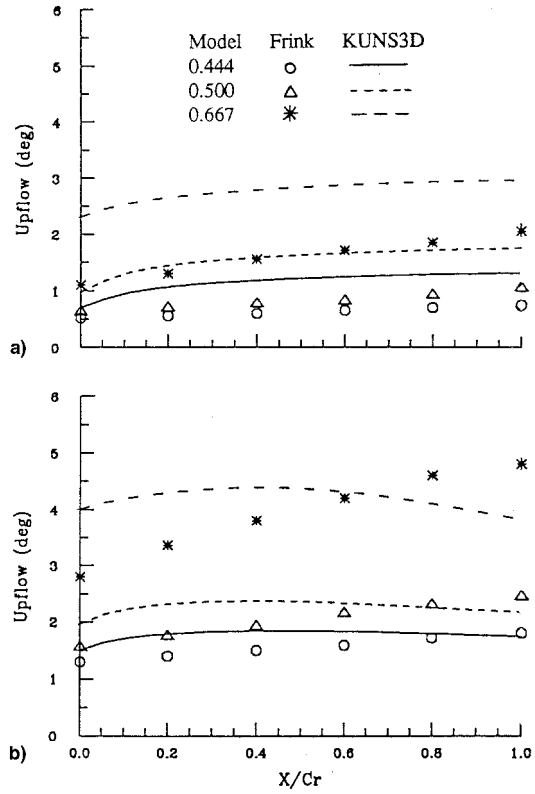


**Fig. 4 Effect of model-to-tunnel span ratios on the induced streamline curvature for a 65-deg delta wing in a 117.4 × 46.96 in. tunnel, $y = 0$, $M = 0.22$. Model scale = wing span/tunnel width ratio. $\alpha$ = a) 15 and b) 30 deg.**

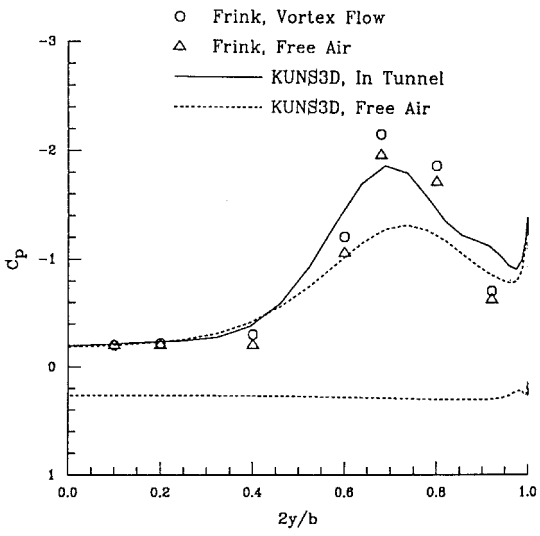


**Fig. 5 Effect of wall interference on the wing surface pressure distributions for a 65-deg delta wing in a 117.4 × 46.96 in. tunnel. $x/c_r = 0.5$, $\alpha = 15$ deg, $M = 0.22$.**

higher in magnitude. However, the streamline curvature effect levels off in the aft portion of the delta wing.

The effect of wall-induced upflow on the wing upper-surface pressure distributions at $\alpha = 15$ deg is shown in Fig. 5. Again, the larger wall-induced effect in the present prediction as seen near the pressure peak region is consistent with the higher predicted induced upflow.

Note that the predicted $C_L$ by Frink's method[14] is typically higher than that by the present method. For example, for the 0.5-sized model $C_L = 0.780$ and 1.630 at $\alpha = 15$ and 30 deg, respectively, as compared with 0.71 and 1.20 by the present method. Wentz's data[25] showed $C_L = 0.66$ and 1.22 at these two $\alpha$. Yet Frink's method[14] predicts lower upflow corrections. This is most likely caused by the effect of viscous wake that is not considered in Frink's method.[14] The viscous wake will deflect downward to cause more interference effect with the tunnel bottom surface.

### Wall Pressure Signature

*65-Deg Delta Wing*

To assess the effect of model sizes, the calculated tunnel wall pressure distributions for three different-sized models (span/tunnel-width ratio of 0.444, 0.5, and 0.667) are presented in Fig. 6. It is seen that for all models the wall static pressure patterns are relatively similar around the model. Two nonuniform regions are seen with one on the floor under the wing, which indicates that the interference effect is caused mainly

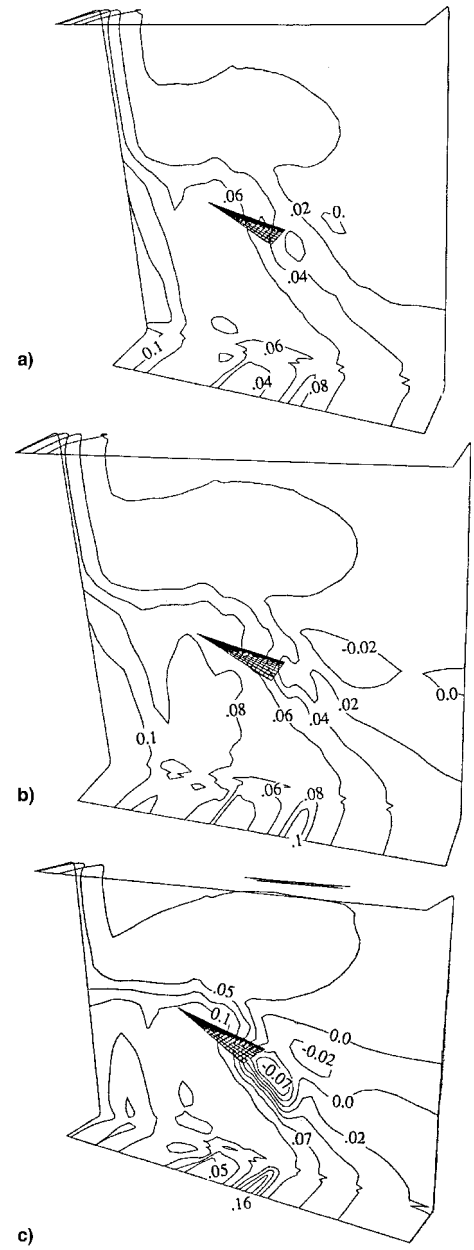


**Fig. 6 Tunnel wall static pressure distribution predicted by the present method for 65-deg delta wings in a 117.4 × 46.96 in. tunnel at $\alpha = 30$ deg and $M = 0.22$. Model scale = wing span/tunnel width ratio. Model scale a) 0.444, b) 0.500, and c) 0.667.**

by wake blockage. The large model has higher pressure difference in this region, implying higher blockage. The other nonuniform region is on the side wall; this is caused by the high model span-to-tunnel width ratio. The large model apparently has more significant influence on the side wall than the other two models, being exhibited by the larger vortical pattern on the wall. The small and medium models induce a similar pattern of wall pressure distribution as that of the large model on both the floor and side wall, only with a reduced magnitude of the pressure coefficient. The ceiling pressure distribution is uniform for all three cases. The wall $C_p$ distribution is positive below the model and is reduced downstream, which means the main interference effect is mainly caused by the induced flow upwash. For the conventional pressure signature methods, the measurements are usually taken on the tunnel ceiling and floor either along the centerline[9] or several streamwise rows.[11] As indicated in Fig. 6c, at high lift there should be more measuring points on the floor and also on the side wall around the model.

*Wing–Body–Strake Configuration*

This model was the one tested in NASA Langley Research Center's 7 by 10 ft wind tunnel with a sting support.[26] The model has a cylindrical body with a 44-deg swept wing and a medium-size leading-edge extension (strake). The flow conditions selected for the present study are $M = 0.3$ and $Re = 1.3 \times 10^6$. Figure 7 shows the calculated tunnel wall pressure distributions for both the original model and a model size equal to 1.5 times larger than the original one. It is seen that for the original model the wall static pressure is relatively uniform and symmetrical around the model. The only nonuniform region is on the floor in the wake region where the sting should contribute a significant part of the interference effect. The implication of this is that the interference effect will be mainly blockage, not upflow variation. On the other hand, the large model induces a $C_p$ distribution that is more positive below the model. This means the main interference effect will be more because of the flow upwash change, not blockage.[27] Based on this assessment, it is seen that at high lift the area on the floor in the near wake should be emphasized in pressure measurement in a pressure signature method.

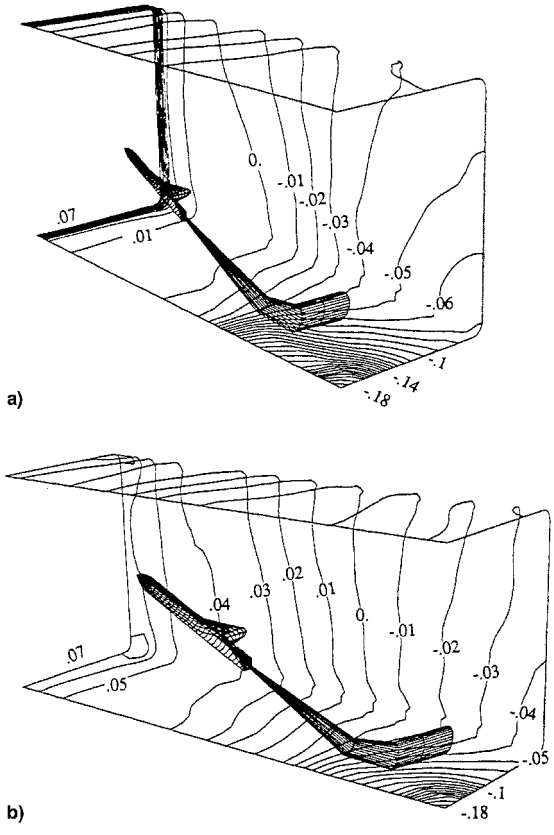


**Fig. 7 Tunnel wall static pressure distribution predicted by the present method for a wing-body-strake model in a 7 × 10 ft tunnel at α = 25 deg and $M = 0.3$: a) original size model (scale = 1.0) and b) large model (scale = 1.5).**

**Wall Interference Corrections**

Based on the consideration of momentum principle, an average $\Delta\alpha$ in the far field computed over the wake region near the center plane is used to correct both the upflow and streamline curvature effects. For a delta wing, it is taken in a plane at the end of the grid system. Average $u$ is taken over the whole plane at the model trailing edge. However, to avoid any direct sting effect, this average value of $\Delta\alpha$ is taken in a plane at the end of the aft body when a sting is present. Average $u$ is taken over the whole plane at the body tail. Results of wall

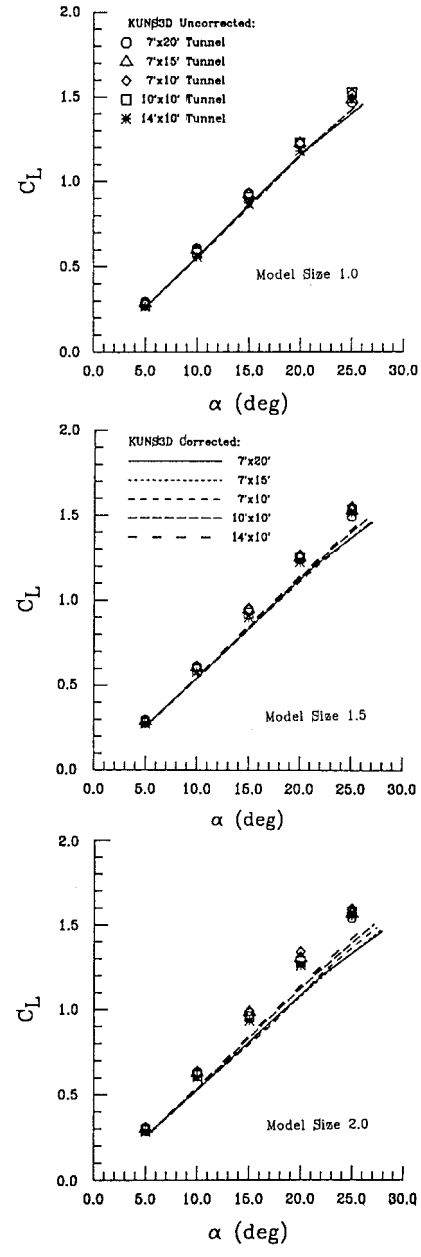


**Fig. 8 Effect of tunnel sizes on wall interference corrections for the wing–body–strake model of different scales at $M = 0.3$. Model size is defined as the linear enlargement of the original model.**

corrections for a delta wing were reported in Ref. 17 and will not be repeated here.

To develop correction charts for wall interference, extensive computational study with the wing–body–strake model of different sizes in different assumed tunnels was conducted.[28] A successful correction method was regarded as the one that could reduce all of these results into one single curve. In addition to the original 7 × 10 ft tunnel, four geometrically extrapolated tunnel sizes, 7 × 20 ft, 7 × 15 ft, 10 × 10 ft, and 14 × 10 ft, were also used. The *H*/*W* ratios represented by these five tunnels were therefore, 0.35, 0.47, 0.7, 1.0, and 1.4. For each of the four additional tunnels, a series of calculations was carried out for all three model sizes, i.e., model scales of 1.0, 1.5, and 2.0. The obtained results were used as the database from which the correction charts are derived. However, because of the lengthy computing time, only one Mach number was investigated. Only some of these results will be presented.

Figure 8 shows the results for these three different models. It is seen that with a model size of scale 1.5 or less, the corrected curves are quite consistent. As the model size is increased to a scale of 2.0, the corrections are less consistent, perhaps because the flowfield around a larger model may be fundamentally changed by wall interference. It is also seen that the correction is consistently reduced with increased tunnel *H*/*W* ratios.

To derive the correction charts based on the aforementioned calculations, the wall-induced upflow corrections are summarized in Fig. 9 for three model sizes in five tunnels. As seen in the figure, increasing the model size increases the upflow correction consistently for all of the tunnels simulated. In most cases it is also nearly linear with increasing angles of attack. Increasing the *H*/*W* ratio is seen to be favorable in reducing

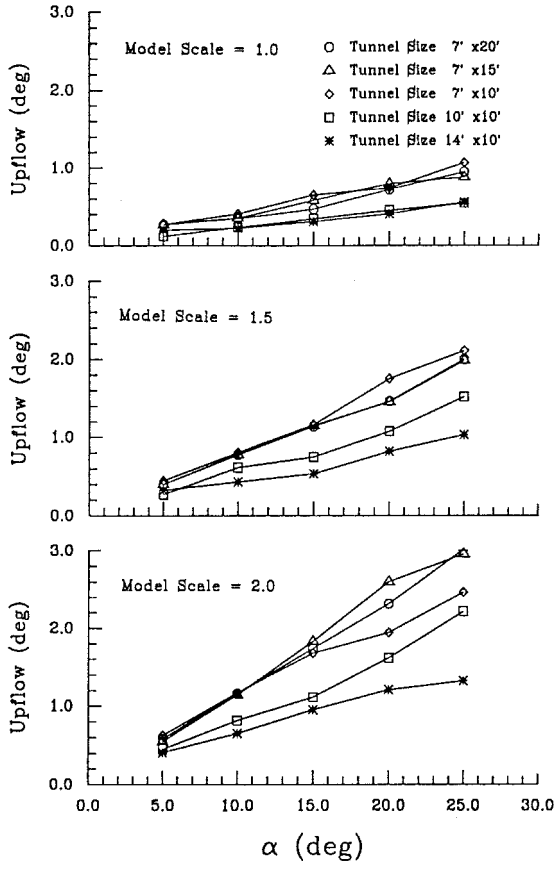


**Fig. 9 Effect of tunnel sizes on the wall-induced upflow corrections for the wing–body–strake models of different size at *M* = 0.3. Model size is defined as the linear enlargement of the original model.**

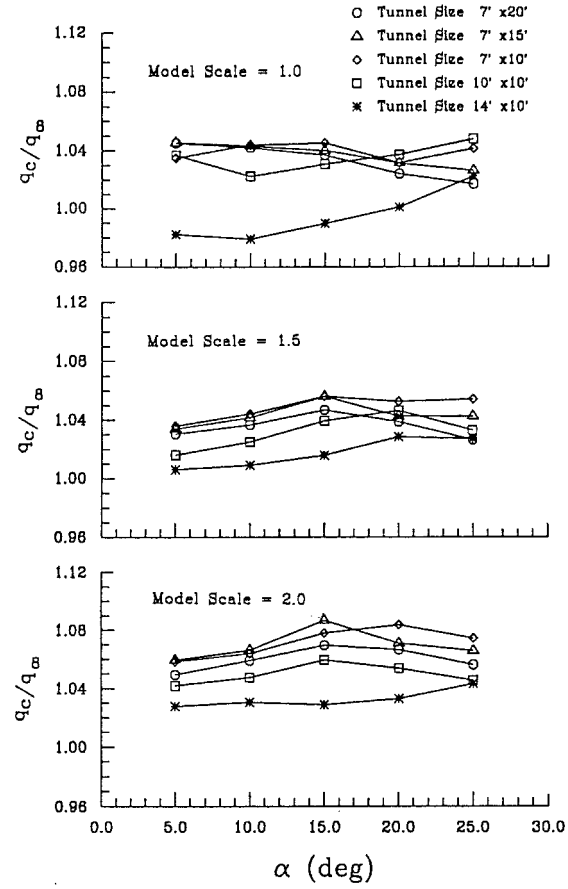


**Fig. 10 Effect of tunnel sizes on the wall-induced blockage corrections for the wing–body–strake models of different size at *M* = 0.3. Model size is defined as the linear enlargement of the original model.**

the amount of correction. This is especially true for larger models.

The blockage effect is shown in Fig. 10. The corrections do not vary as much with respect to the angle of attack for the blockage as compared to the upflow corrections. The effect of model size is again seen to increase the amount of corrections, with only a few exceptions. These apparent exceptions may be because of the nonlinearity of vortex flow. The most significant effect is seen to be for cases with the highest *H*/*W* ratio (i.e., 14 × 10 ft tunnel). The correction for this tunnel is consistently the lowest one in all cases. The variation in the curves for cases with smaller *H*/*W* ratios (i.e., 7 × 15 ft and 7 × 20 ft tunnels) is more complicated. However, the differences between the corrections for cases with different tunnel width is not dramatic.

### Wall Interference Correction Charts

The upflow correction was shown to be nearly linear for all of the cases studied. An interference correction parameter is defined as

$$\mathrm{ICP} = (S/C)/(H/W) \tag{6}$$

where *S*/*C* is the blockage ratio of the model wing planform area to the tunnel cross-sectional area, and *H*/*W* is the tunnel height-to-width ratio. Four curves with different ICPs are generated in the upflow correction chart as shown in Fig. 11. The correction is correlated with the uncorrected α because it is more appropriate to use α than $C_L$ when vortex flow is present. For a given test model, the correction factor can be obtained by interpolation. For an ICP value slightly greater than 0.091,

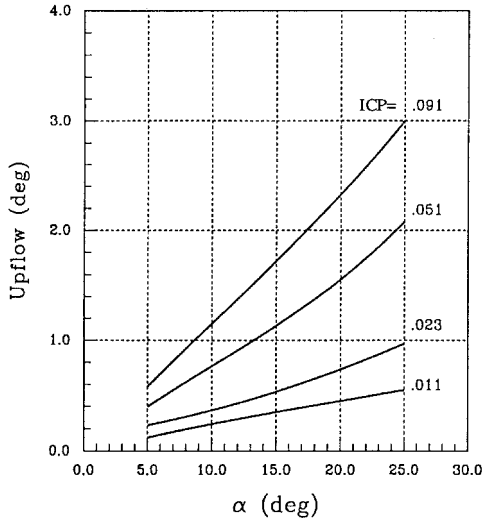


**Fig. 11 Chart for the upflow corrections.**

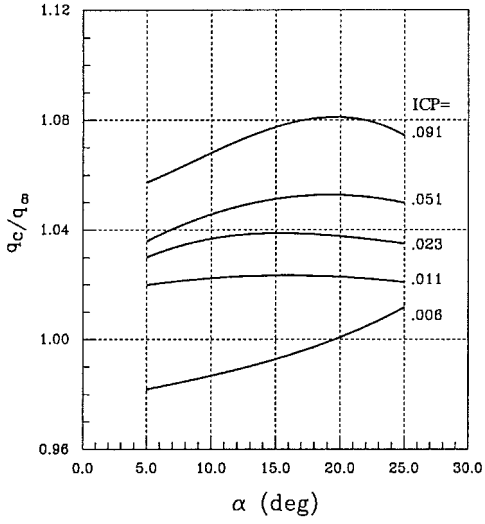


**Fig. 12 Chart for the blockage corrections.**

the top curve should be used. Note that the present chart is valid only before vortex bursting.

The blockage correction in the present study appears to be more complicated for the tunnel-size effect. On the other hand the model-size effect on the blockage correction is relatively simple for the different-sized models simulated in a given wind tunnel. In all cases except one, the variation in blockage effect is not dramatic with respect to the change in angle of attack. The exceptional case is the one with a scale-1.0 model simulated in the tunnel with the largest $H/W$ ratio, which shows increased blockage corrections with respect to the angle of attack. By using the same correction parameter, ICP, the best approximation to correlate these blockage correction curves can be obtained. For the correction chart shown in Fig. 12, five curves are derived from the computed results based on the five different correction parameters. Interpolation among these curves should be sufficient for common wind-tunnel sizes.

To illustrate the application of these two correction charts, test results for a 76-deg delta wing model in the 28 × 40 in. BART tunnel at NASA Langley Research Center[29] will be corrected. The model was tested at $M = 0.2$ and $Re = 10^6$ based on the root chord. The wing area was 81 in.$^2$. The results are compared with the lift curves obtained from various wind tunnels in Fig. 13. The agreement of the present corrected curve with others is seen to be good. In Ref. 29 the corrections based

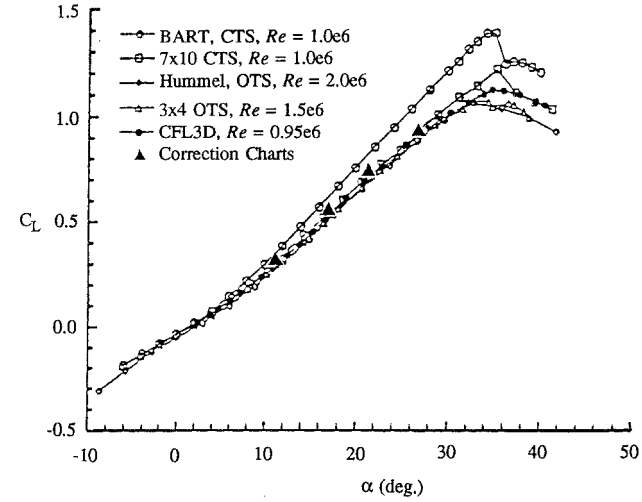


**Fig. 13 Lift curves for a 76-deg delta wing model tested in various tunnels obtained from Ref. 29, and corrections of BART tunnel data from the present correction charts.**

on the conventional attached-flow theory were shown to be much smaller.

## Conclusions

The upwash and blockage corrections induced by wall interference were investigated based on the thin-layer Navier–Stokes solutions. The interference assessment was performed by first calculating the static pressure distribution on the wall with the model in the tunnel. Then the model was removed and the interference flowfield was calculated using the computed wall pressures as the boundary condition. The correction was applied to the wind-tunnel longitudinal aerodynamic data to account for the wall effects. The wake deflection effect and flow separation characteristics that could not be accounted for by the potential-flow methods were treated adequately by the $N$–$S$ solver. Results for a 65-deg delta wing were compared with the free-vortex-sheet results and showed good agreement in trend for the effect on aerodynamic twist at $x/c_r = 0.5$ and effect on the streamline curvature at $y = 0$. The present method predicted a higher upflow correction in magnitude by properly treating the wake interference. A wing–body–strake configuration of different model sizes was numerically simulated in rectangular tunnels of different sizes at $M = 0.3$. Two correction charts for the upflow and blockage corrections were derived from these calculations. These charts should be applicable to configurations with vortex flow and were successfully applied to a 76-deg delta wing.

## References

[1]Silverstein, A., and White, J. A., "Wind-Tunnel Interference with Particular Reference to Off-Center Positions of the Wing and to the Downwash at the Tail," NACA Rept. 547, 1935, pp. 135–147.

[2]Rae, W. H., Jr., and Pope, A., *Low Speed Wind Tunnel Testing*, Wiley, New York, 1984, pp. 344–444.

[3]Garner, H. C., Rogers, E. W. E., Acum, W. E. A., and Maskell, E. C., "Subsonic Wind Tunnel Wall Corrections," AGARDograph 109, Oct. 1966.

[4]Joppa, R. G., "A Method of Calculating Wind Tunnel Interference Factors for Tunnels of Arbitrary Cross Sections," NASA CR-845, July 1967.

[5]Joppa, R. G., "Wind Tunnel Interference Factors for High Lift Wings in Closed Wind Tunnel," NASA-CR 2191, Feb. 1973.

[6]Doberenz, M. E., "Wind Tunnel Interference Factors for High Lift Wings in Open Jet Wind Tunnel," Project Rept. 74-18, Von Kármán Inst. for Fluid Dynamics, Belgium, 1974.

[7]Maskell, E. C., "A Theory of the Blockage Effects on Bluff Bodies and Stalled Wings in a Closed Wind Tunnels," British Aeronautical Research Council, R & M 3400, 1963.

[8]Pass, C. Q., "A Wake Blockage Correction Method for Small Subsonic Wind Tunnels," AIAA Paper 87-0294, Jan. 1987.

[9]Hackett, J. E., Wilsden, D. J., and Stevens, W. A., "A Review of the Wall Pressure Signature and Other Tunnel Constraint Correction Methods for High Angle-of-Attack Tests," AGARD-R-692, Feb. 1981.

[10]Proctor, J. G., "Wall Pressure Signature Wind-Tunnel Wall-Constraint Correction Methods," British Aerospace, BAe-ARG-188, April 1984.

[11]Ashill, P. R., and Keating, R. F. A., "Calculation of Tunnel Wall Interference from Wall-Pressure Measurements," *Aeronautical Journal*, Vol. 92, Jan. 1988, pp. 36–53.

[12]Lee, K. D., "Numerical Simulation of the Wind Tunnel Environment by a Panel Method," *AIAA Journal*, Vol. 19, No. 4, 1981, pp. 470–475.

[13]Johnson, F. T., and Rubbert, P. E., "Advanced Panel-Type Influence Coefficient Methods Applied to Subsonic Flow," AIAA Paper 75-50, Jan. 1975.

[14]Frink, N. T., "Computational Study of Wind-Tunnel Wall Effects on Flow Field Around Delta Wings," AIAA Paper 87-2420, Aug. 1987.

[15]Rizk, M. H., and Smithmeyer, M. G., "Wind-Tunnel Wall Interference Corrections for Three-Dimensional Flows," *Journal of Aircraft*, Vol. 19, No. 6, 1982, pp. 465–472.

[16]Vatsa, V. N., and Wedan, B. W., "Effect of Sidewall Boundary Layer on a Wing in a Wind Tunnel," *Journal of Aircraft*, Vol. 26, No. 2, 1989, pp. 157–161.

[17]Thomas, J. P., and Lan, C. E., "The Simulation and Correction of Wind Tunnel Wall Interference on Delta Wing Lift Using Navier-Stokes and Euler Solutions," AIAA Paper 91-3300, Sept. 1991.

[18]Lan, C. E., and Hsing, C. A., "Assessment and Correction of Tunnel Wall Interference by Navier-Stokes Solutions," International Council of the Aeronautical Sciences, 92-3.5.2, May 1992.

[19]Lefebvre, A. H., "A Method of Predicting the Aerodynamic Blockage of Bluff Bodies in a Ducted Airstream," College of Aeronautics, Rept. Aero-188, Cranfield, England, UK, 1965.

[20]"Blockage Corrections for Bluff Bodies in Confined Flows," Engineering Sciences Data Unit, Item 80024, London, 1980.

[21]Chambers, J. R., "High-Angle-of-Attack Aerodynamics: Lessons Learned," AIAA Paper 86-1774, June 1986.

[22]Pulliam, T. H., "Euler and Thin Layer Navier Stokes Codes: ARC2D, ARC3D," Computational Fluid Dynamics User's Workshop, Univ. of Tennessee Space Inst., Tullahoma, TN, March 1984.

[23]Balwin, B. S., and Lomax, H. "Thin Layer Approximation and Algebraic Model for Separated Turbulent Flows," AIAA Paper 78-257, Jan. 1978.

[24]Lindeberg, T., "The Construction of a Three-Dimensional Finite Volume Grid Generator for a Wing in a Wind Tunnel with Application to Navier-Stokes Flow Solvers," Aeronautical Research Inst. of Sweden, FFA-TN-1987-58, Oct. 1987.

[25]Wentz, W. H., and Kohlman, D. L., "Wind Tunnel Investigations of Vortex Breakdown on Slender Sharp-Edged Wings," NASA CR-98737, Nov. 1968.

[26]Luckring, J. M., "Subsonic Longitudinal and Lateral Aerodynamic Characteristics for a Systematic Series of Strake-Wing Configurations," NASA TM 78642, Feb. 1979.

[27]Crites, R. C., "Transonic Wind Tunnel Boundary Interference — A Correction Procedure," CP 429, AGARD, Sept. 1987 (Paper 15).

[28]Hsing, C. C., "A Computational Method for Wind Tunnel Wall Corrections Based on Navier-Stokes Solutions," Ph.D. Dissertation, Univ. of Kansas, Lawrence, KS, May 1994.

[29]Washburn, A. E., "The Effect of Freestream Turbulence on the Vortical Flow over a Delta Wing," M.S. Thesis, George Washington Univ., Washington, DC, Dec. 1990.